

# Chapter 14

## Strategies for Improving the Comparison of Frequency Response Functions with Similarity Metrics



Hunter R. Kramer, Levi H. Manring, John F. Schultze, Sandra J. Zimmerman, and Brian P. Mann

**Abstract** Determining the similarity of an existing structure with a reference structure is an important problem in structural dynamics. For this purpose, many metrics have been developed to quantify the similarity of frequency spectra, such as two transfer functions. However, these approaches yield an aggregate or single numerical score for the similarity over an entire frequency range. This paper, instead, applies these common similarity metrics across a range of frequencies and plots the results to illustrate instances where counterintuitive results can occur. For example, the highest degree of similarity often occurs at a frequency where the two frequency spectra appear to diverge.

The result is that counterintuitive cases can be corrected by applying a log frequency shift to the response, enabling better comparisons. Additionally, a similarity metric that compares the phase of the frequency spectra can be applied to make further comparisons. This paper seeks to verify the new methods presented in Manring et al. (*J Sound Vib* 539:117255, 2022) using a modified experiment and proposes a windowing method as another tool for comparing similar transfer functions. The authors investigate these approaches while applying historical measures of similarity, to provide a more intuitive result for a similarity score. While the shifted frequency spectra can now provide more intuitive comparisons of the degree of similarity, the degree of shifting the frequency segments provides an additional opportunity to quantify the differences in the frequency spectra. The developed approaches were applied to both theoretical and experimental systems.

**Keywords** Frequency response · Vibration · Metric · Log frequency shift · Phase similarity metric

### 14.1 Introduction

In the field of engineering and design, there are numerous applications of random vibration testing. Industries such as automotive, aerospace, and manufacturing leverage their understanding of vibrations to study critical system dynamics and increase the robustness of designs. One common way of capturing the dynamics of a vibrating system is to measure its frequency response function (FRF). FRFs are a measure of system behavior in response to some external force. FRFs are unique to classes of systems and comparing similar FRFs can exemplify key differences between the systems in question.

Tools that quantitatively compare FRFs are commonly referred to as similarity metrics. These metrics take two FRF signals, one for reference and one for comparison, and compare the value of the FRFs at each spectral line. Using this data, the metrics compute a single value that describes the similarity between them. There are several methods by which this can be done, such as the use of scaled inner products. This type of method is especially useful at comparing the amplitudes of two FRFs and has the added benefit of producing a normalized value between 0 and 1 (0 being least similar and 1 being most similar).

---

H. R. Kramer (✉) · L. H. Manring · B. P. Mann

Department of Mechanical Engineering and Materials Science, Pratt School of Engineering Duke University, Durham, NC, USA  
e-mail: [hunter.kramer@duke.edu](mailto:hunter.kramer@duke.edu); [levi.manring@duke.edu](mailto:levi.manring@duke.edu); [brian.mann@duke.edu](mailto:brian.mann@duke.edu)

J. F. Schultze · S. J. Zimmerman

Los Alamos National Laboratory, Los Alamos, NM, USA  
e-mail: [schultze@lanl.gov](mailto:schultze@lanl.gov); [zimmerman@lanl.gov](mailto:zimmerman@lanl.gov)

The use of scaled inner products can be seen in the frequency response assurance criterion, or FRAC [1] which is given by

$$\text{FRAC} = \frac{|\sum_{k=1}^{N_k} [\mathbf{H}_A(f_k)^H \cdot \mathbf{H}_B(f_k)]|^2}{\sum_{k=1}^{N_k} [\mathbf{H}_A(f_k)^H \cdot \mathbf{H}_A(f_k)] \sum_{k=1}^{N_k} [\mathbf{H}_B(f_k)^H \cdot \mathbf{H}_B(f_k)]} \quad (14.1)$$

where  $\mathbf{H}_A$  is the reference FRF,  $\mathbf{H}_B$  is the comparison FRF,  $N_k$  is the number of spectral lines to compare, and  $f_k$  is the frequency at spectral line  $k$ . The superscript  $H$  indicates the Hermitian transpose of the preceding vector. The FRAC excels at comparing the amplitude of two FRFs but is prone to scaling issues. To remedy this a modified version of FRAC, called MFRAC, scales the result by the ratio of minimum to maximum powers for each FRF.

Some similarity metrics utilize other methods besides scaled inner products. The magnitude-shape similarity function (MSSF) is a combined comparison metric that compares not only magnitude but phase information [2]. One unique feature of MSSF is its use of the hyperbolic tangent function. For this paper, only the magnitude comparison of MSSF will be studied, which is called  $M_\alpha$  and is given by

$$M_\alpha(f) = 1 - \tanh\left(\frac{\ln(3) |20 \log_{10} |H(f)||}{2\alpha}\right). \quad (14.2)$$

$M_\alpha$  uses a scaling factor  $\alpha$  and a complex transfer function between two FRFs  $H(f)$ , as opposed to a scaled inner product.

Another interesting metric is the frequency response function similarity metric (FRFSM) [3]. This method differs from the previous metrics in its use of a probability density function to compare decibel scaled magnitudes of two FRFs. The process of using FRFSM is done using three equations. The first is the probability density function given by  $g$  as

$$g(x, \mu, \sigma^2) = \frac{1}{\sigma\sqrt{2\pi}} \exp\left(-\frac{1}{2} \left(\frac{x - \mu}{\sigma}\right)^2\right) \quad (14.3)$$

wherein  $\sigma$  is the standard deviation,  $x$  is the variable of interest, and  $\mu$  is the mean. The next equation is  $\epsilon$  which describes the decibel scaled magnitude of the two FRFs of interest given as

$$\epsilon(f) = \left|10 \log_{10} \|\mathbf{H}_A(f)\|^2 - 10 \log_{10} \|\mathbf{H}_B(f)\|^2\right|. \quad (14.4)$$

In Eq. 14.4,  $f$  is the frequency where the FRF signals are being applied. The final expression for FRFSM is given by

$$\text{FRFSM}(f) = \frac{g(\epsilon(f), 0, \sigma_0^2)}{g(0, 0, \sigma_0^2)}. \quad (14.5)$$

In Eq. 14.5, the mean  $\mu$  is taken to be 0 for both probability density functions. Additionally,  $\sigma_0^2$  is a reference value used to scale the metric. This value was recommended to be 6 dB by the authors of [3].

Up to this point, we have only described metrics that compare the amplitudes of FRFs with no consideration of phase. There exist several metrics that include or specifically study phase, but this paper focuses on the phase similarity metric (PSM) [4]. This metric, which is based on FRFSM, utilizes the probability density function  $g$  with one key difference. PSM introduces the phase error metric,  $\angle H_w$ , defined as

$$\angle H_w = |W(\angle H_e)| \quad (14.6)$$

where  $H_e$  is the difference between the phases of the two FRFs and  $W$  is a function that wraps the resultant phase from  $-\pi$  to  $\pi$  radians. The equation for PSM then follows the form of FRFSM, given by

$$\text{PSM}(f) = \frac{g(\angle H_w, 0, \sigma_0^2)}{g(0, 0, \sigma_0^2)}. \quad (14.7)$$

To properly scale the result from Eq. 14.7 between 0 and 1, the value of  $\sigma_0^2$  was chosen to be  $\pi/4$  by the authors of [4].

One method by which the previously discussed metrics can be made more useful is the log frequency shifting (LFS) method [4]. This method can be used to shift the FRF of a comparison signal linearly in the frequency domain to resemble a reference signal more closely. This can be particularly useful because many different factors can shift the relevant features, such as the resonant frequencies of FRFs. This can lead to inaccurate comparisons of similar signals or even signals from the same system. This method can be used in two ways, using a single shift or using several different shifts centered around the resonant frequencies of the reference FRF. This paper applies a single shift to align similar FRFs. An in-depth description of how this method works can be found in reference [4].

## 14.2 Simulation

This section applies the previously described metrics to an idealized system. For this study, an Euler-Bernoulli beam with point excitation and point measurement was analyzed. The excitation and measurement were both located at the end of the beam to produce and capture a large system response. The beam characteristics used in this study are representative of the beam used in the later Experimental Validation section. The simulation parameters used are listed in Table 14.1 of the Appendix.

The LFS technique is useful in aligning signals that have similar features but may be shifted in the frequency domain. To demonstrate this technique, the beam response was simulated for various lengths. The equation for the resonant frequencies of an Euler-Bernoulli beam is

$$\omega_n = \sqrt{\frac{EI}{\rho A}} \beta_n^2 \quad (14.8)$$

where  $\omega_n$  is the resonant frequency,  $E$  is the Young's modulus,  $I$  is the area moment of inertia,  $\rho$  is the beam density, and  $A$  is the cross-sectional area [5]. The value of  $\beta_n$  can be attained by solving the transcendental equation for an Euler-Bernoulli beam with fixed-free boundary conditions.

By changing the beam length by some constant,  $\gamma$ , we can alter the resonant frequencies of the beam by a measurable amount. Rearranging Eq. 14.8 slightly gives

$$\omega_{n,\gamma} = \sqrt{\frac{EI}{\rho A(\gamma L)^4}} (\beta_n L)^2 \quad (14.9)$$

which allows us to see this behavior directly [4]. In Eq. 14.9,  $L$  is the beam length. For the  $n$ th value of  $\beta_n L$ , it becomes evident that the resonant frequency  $\omega_{n,\gamma}$  will change as a factor of  $1/\gamma^2$  (assuming the other variables are constant). Applying linearly spaced values of  $\gamma$  to our beam produces linearly spaced FRFs, perfect for demonstrating the LFS technique. Figure 14.1 shows these FRFs plotted on a log scale for the first three resonant frequencies. Note that the magnitude of these FRFs is dimensionless throughout this paper.

Upon visual inspection, these FRFs are clearly similar. This is more difficult to describe mathematically, as historical metrics of FRF comparison can lack visual intuition. These metrics are generally applied using one of two methods. The first method is to compare signals over the entire frequency spectra giving a single, overall score of similarity. The second is by applying the metric at each spectral line, called the "point-to-point" method. While this is more useful in some cases, it ignores the overall behavior of the curves in question. Thus, applying classic FRF comparison metrics in these ways can often be misleading. For example, consider two of the signals from Fig. 14.1 that are shown in Fig. 14.2a. If the FRFs for gamma values of  $\gamma = 1.0$  (reference) and  $\gamma = 1.05$  are compared using the similarity metric FRFSM without LFS, the results are very confusing. To elaborate, the FRFSM provides a value of unity between the resonant frequencies. Conversely, while near the resonant frequencies, the value varies. One way to mitigate this effect is to use a windowed approach. This approach applies the desired comparison metric to a window of a predetermined size that shifts from the beginning to the end of the signal. This provides a "middle ground" between the single score and point-to-point methods. Figure 14.2 gives the FRFSM score between the two FRFs for varying window sizes.

A few more notable behaviors can be observed in Fig. 14.2. One is that all these similarity metrics are at a maximum at the points where the FRFs cross paths. This makes sense mathematically because the value of the FRFs is equal to the corresponding frequencies. This result falls victim to the metrics' lack of intuition, however, because the FRFs are diverging

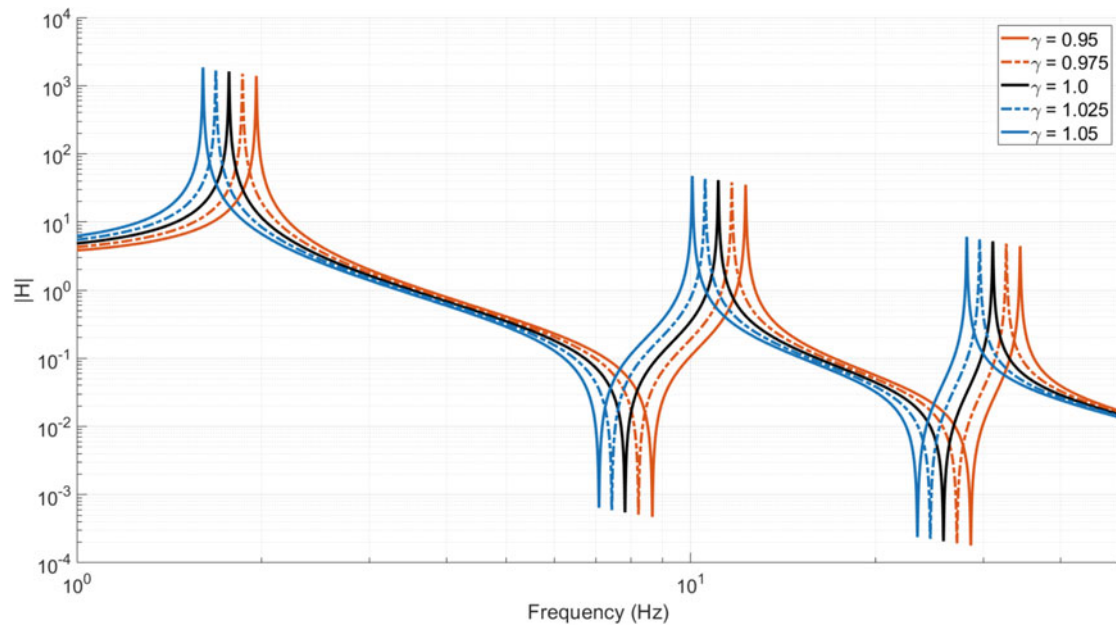


**Fig. 14.1** The FRFs for simulated Euler-Bernoulli beams of differing length

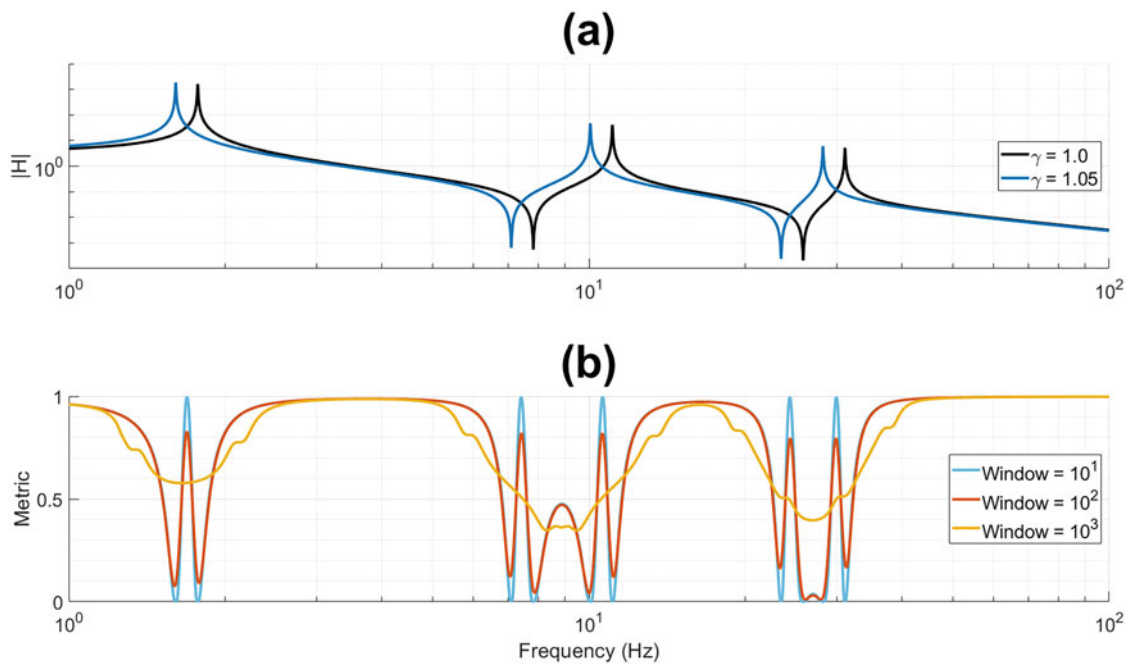


**Fig. 14.2** A demonstration of the advantages of using a windowed approach with varying window sizes. (a) shows the FRF amplitudes for  $\gamma = 1.05$  and the baseline FRF. (b) shows the performance of FRFSM on the reference signal and the baseline signal using various window sizes

at these points. By varying the selected window size, a different result can be seen. In Fig. 14.2 three window sizes are used:  $10^1$ ,  $10^2$ , and  $10^3$  spectral lines. Note that the frequencies simulated in this study are spaced on a logarithmic scale as opposed to a linear scale. This ensures that the effect of the window size is applied evenly to logarithmically scaled spectra. As the window size increases, the sensitivity of the applied metrics decreases. This can be useful for attenuating out sharp spikes in the signal but can also cause the metric to be insensitive to important behaviors. The extreme case of this is in the single score method, where the window size is equal to the size of the FRF, leading to one comparison value. In Fig. 14.2, a window size of  $10^2$  is a good compromise as it preserves the rises and falls of the metric without excessive peaks or attenuation. For the remainder of this section, the figures use this window size when calculating similarity metrics.

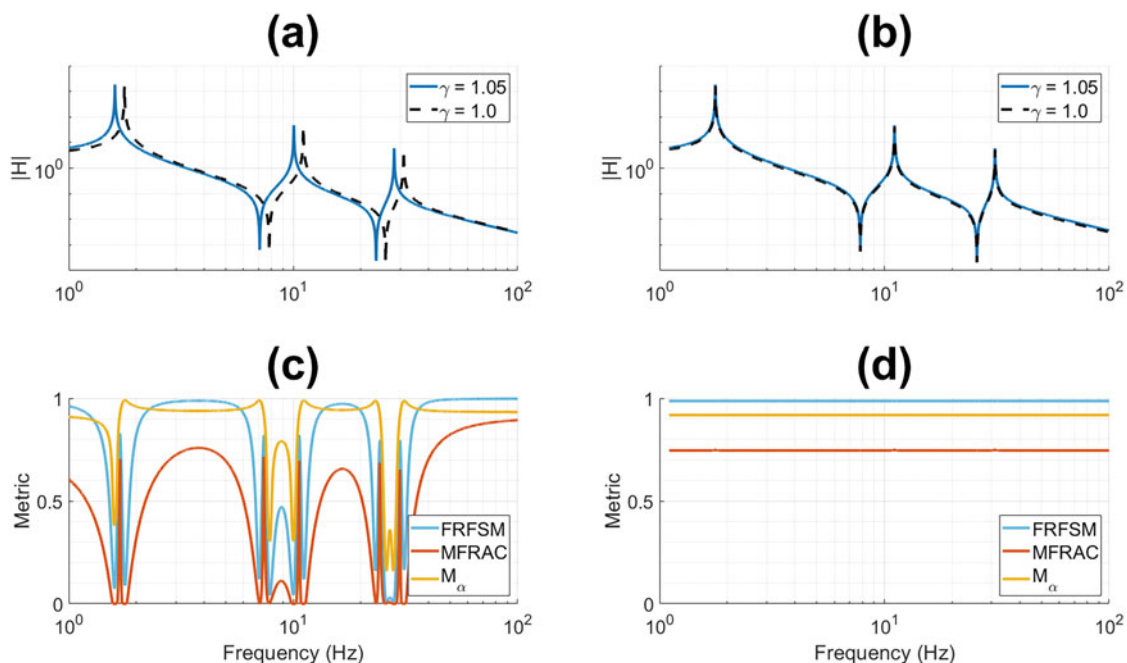


**Fig. 14.3** An amplitude comparison of the FRFs for  $\gamma = 1.05$  and the reference FRF. (a) shows the comparison FRF for  $\gamma = 1.05$  and the baseline FRF. (b) shows the LFS comparison and reference FRFs. (c) shows the performance of several metrics applied to the non-shifted FRFs. (d) shows the performance of the shifted FRFs

In conjunction with windowing, LFS can be utilized to further improve these mathematical comparisons. Figure 14.3 shows the three different comparison metrics, MFRAC, FRFSM, and  $M_\alpha$ , applied to the two FRFs from Fig. 14.2a.

Applying the similarity metrics before log shifting results in some useful information. Like the previous case, the metrics represent the similarity well between the resonant frequencies but perform with varying accuracy near them. Once the reference FRF is log shifted, all three metrics become constant. FRFSM becomes nearly unity, showing an almost perfect correlation, while  $M_\alpha$  and particularly MFRAC are lower in value. This is due to how MFRAC scales its value by the ratio of the maximum to minimum powers. From this analysis, it can be concluded that LFS is beneficial in the comparison of amplitudes of FRF functions.

Another useful tool in FRF comparisons is to compare the phase. Historically, there are a limited number of metrics that include the phase as part of the comparison. This paper studies the phase similarity metric or PSM [4]. PSM is successful in capturing the phase behaviors of the comparison signal about the reference. This metric has been applied to the two FRFs from Fig. 14.2a and can be seen in Fig. 14.4c. To further enhance the comparison, LFS can be applied to align the phase shifts of the signals. The resulting curve can be seen in Fig. 14.4d.

As with the amplitude comparison, a few notable behaviors can be observed. Before LFS, the PSM metric is near unity for most of the signal. Large jumps in the metric occur at the phase shifts, however, because of the slight delay that increasing the length creates. After applying LFS, the signals are aligned such that the curves are indistinguishable. As a result, the PSM metric becomes constant and attains a value of unity. Figure 14.4 exemplifies the advantages of using LFS in conjunction with PSM. Applying LFS allows for the PSM metric to provide a more useful result in contrast to when it is used alone.

### 14.3 Experimental Validation

In the previous section, the LFS method and PSM were applied to the simulated response of a beam (in Figs. 14.3 and 14.4, respectively). This section applies these methods to test data from a simple experimental setup. Figure 14.5 shows a picture of the experimental system. An APS dynamics vertical shaker used to study the response of a thin metal beam is shown. The physical characteristics of this beam have been listed in Table 14.2 of the Appendix. To vary the dynamics of this system, an adaptor with an integral magnet was designed to allow for the addition of magnetic weights. A control accelerometer (denoted A) was added to the base of the beam behind the fasteners to capture the movement of the shaker. Additionally,

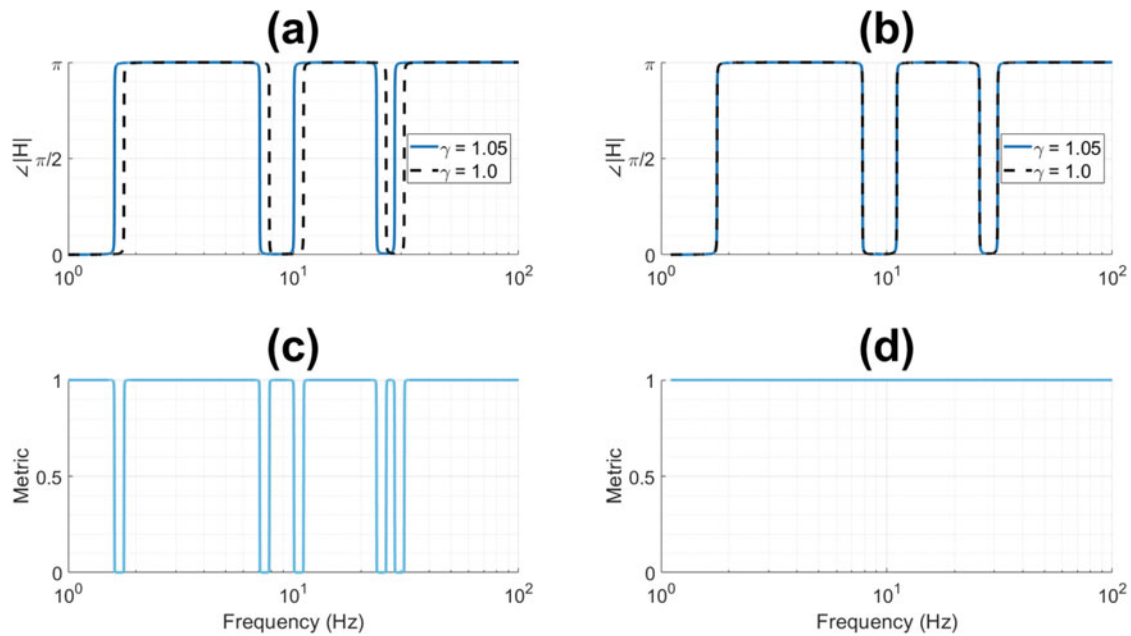


**Fig. 14.4** A demonstration of phase comparison for a reference and comparison FRF. (a) shows the comparison phase for  $\gamma = 1.05$  and the baseline phase. (b) shows the LFS comparison and reference phases. (c) shows the performance of PSM applied to the non-shifted phases. (d) shows the performance of the shifted phase

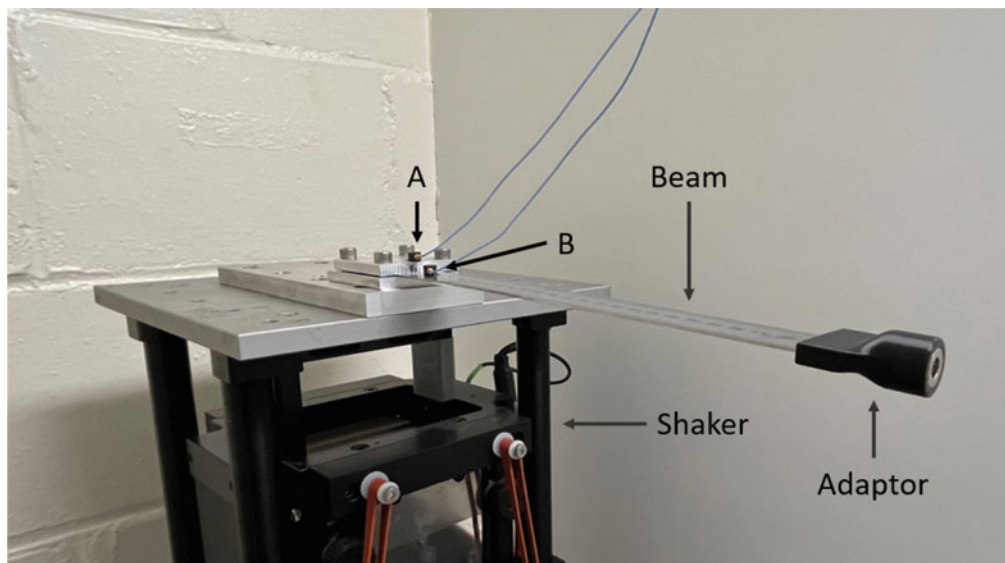


**Fig. 14.5** The experimental fixed-free beam used for validation testing. The setup consisted of two accelerometers (denoted A and B), a vertical shaker, a thin metal beam, and an adaptor with integral magnet to vary the system response

a measurement accelerometer (denoted B) was added in front of the fasteners, directly on the beam to capture the beam's response. This location was chosen to mitigate the system noise incurred during testing. This differed from the simulated case where experimental noise was not considered and thus the response was measured at the end of the beam. An NI PXIe-1082 real-time controller was used with a LabView script to conduct the random vibration testing.

The weights added to the beam had a mass of approximately 9.1 grams each. To get a baseline reading, the beam was first tested without any added mass. Individual masses were then added to the end of the beam and tested using a random vibration study. The masses were approximately 1/6 of the overall mass of the beam. While this is greater than what is commonly used for system perturbations, it is useful for examining extreme cases. From the data collected using the control and measurement accelerometers, the FRF for the system was derived. This was done via a Fourier transform of the time series. Each experimental case consisted of 20 trials, from which the data was averaged and smoothed using Gaussian smoothing.

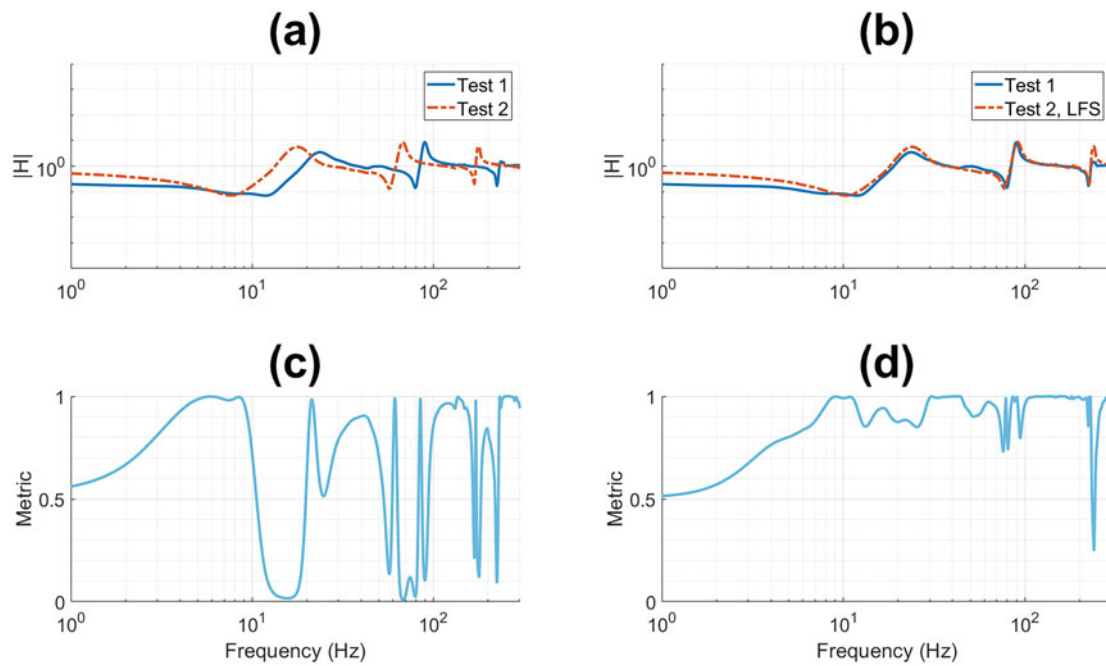


**Fig. 14.6** A comparison of the magnitude of the FRFs for the beam with no added mass (Test 1) and the beam with added adaptor (Test 2). (a) shows the original FRFs. (b) shows the shifted comparison FRF with the original reference FRF. (c) shows the FRFSM applied to the original FRFs. (d) shows the FRFSM applied to the shifted comparison FRF and the original reference FRF

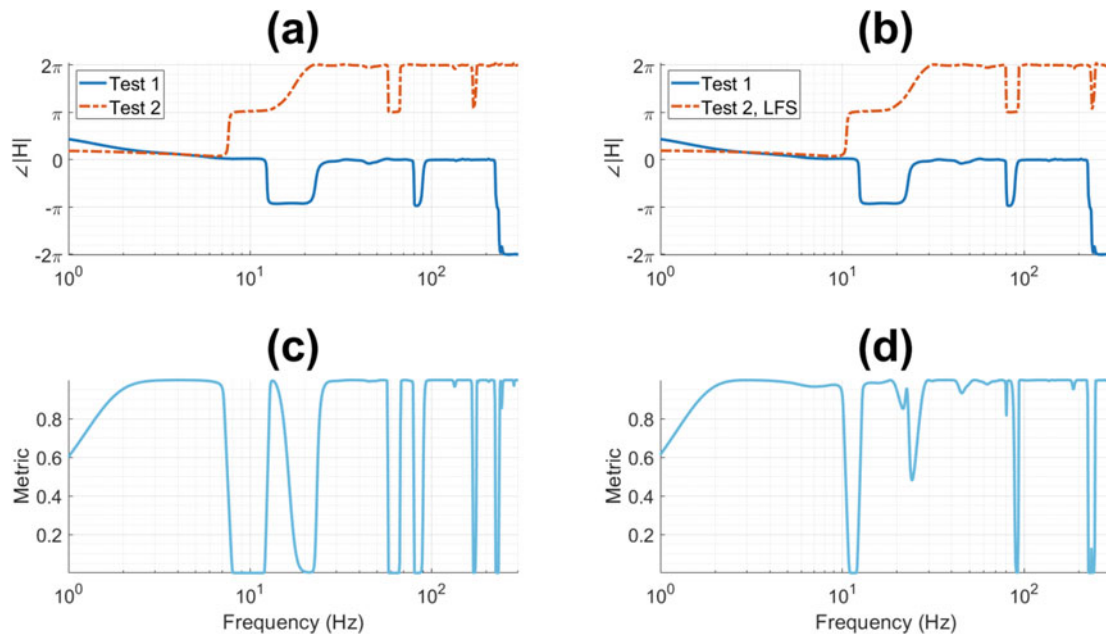


**Fig. 14.7** A comparison of the phase of the FRFs for the beam with no added mass (Test 1) and the beam with added adaptor (Test 2). (a) shows the original FRFs. (b) shows the shifted comparison FRF with the original reference FRF. (c) shows the FRFSM applied to the original FRFs. (d) shows the FRFSM applied to the shifted comparison FRF and the original reference FRF

A comparison of the processed FRFs was done using the LFS and PSM methods. Figure 14.6 shows the results of applying the LFS method to the first and second tests (no mass and 18.8 grams, respectively). Additionally, FRFSM was applied to compare the similarity of the signals before and after LFS.

While the FRFs from these two tests are similar, it can be observed that adding mass to the end of the beam shifts the resonant frequencies down, conversely to our simulated case. The resulting curve from applying FRFSM resembles the simulated case. From the experimental data, however, there is much more variance in general at the location of the resonant frequencies. After the implementation of LFS, the value of FRFSM is close to unity for a majority of the frequencies studied.

The one notable exception is the third resonant frequency. Here, the response from the weighted beam is much greater than from the unweighted beam. When there is no mass, the higher frequency modes dampen out quickly, leading to this result.

Next, the phase of the above FRFs was studied. The phase of the FRFs was unwrapped for clarity and then log shifted using the LFS method. The resultant curves shared similar features but were separated by a shift of  $2\pi$  which can be seen in Fig. 14.7. This shift exemplifies the usefulness of the LFS and PSM methods. While LFS succeeds in aligning resonant frequencies, it still preserves the unique features of each curve.

PSM was then applied to the shifted and unshifted curves. Studying the resulting curves reveals that before LFS there are more jumps between 0 and 1. This makes the signals more difficult to compare and masks the similar features. After applying LFS, the PSM curve still has several jumps between 0 and 1, but they make more sense intuitively. Aligning these features allows for a more direct comparison of the shape of the curves by mitigating the differences caused by the frequency shift. This information is still preserved, however, in the value of the lag factor. The lag factor describes how much the frequency of the comparison FRF must be shifted to align with the reference FRF. This value is derived by maximizing the cross-correlation between the two FRFs, with further details described in [4].

## 14.4 Conclusions

This paper demonstrated the advantages of using the LFS method in conjunction with existing FRF similarity metrics. An Euler-Bernoulli fixed-free beam was simulated with different length parameters to generate similar FRF signals. An experimental beam was studied on a vertical shaker with varying tip masses to validate the LFS method on physical system responses. Similarity metrics were applied to the resulting FRFs of these systems with and without LFS to gain insight into its advantages.

When LFS was applied with the similarity metrics, the results showed a greater correlation between the FRFs. Aligning the peaks of the comparison FRF to the reference FRF leads to more intuitive results while quantifying the shift in the frequency domain. Selecting a suitable window size reduced large peaks in simulation while still preserving important feature information. We find these methods presented in [4] and the proposed windowing method to be beneficial for comparing similar FRFs.

**Acknowledgments** This research is supported by the Delivery Environments program under the Office of Engineering and Technology Maturation at Los Alamos National Laboratory (LA-UR-22-31189).

## Appendix

**Table 14.1** Simulation parameters

Parameter	Symbol	Value	Unit
Young's modulus	$E$	$10^{11}$	N/m <sup>2</sup>
Density	$\rho$	$10^3$	kg/m <sup>3</sup>
Area moment of inertia	$I$	$10^{-12}$	m <sup>4</sup>
Cross-sectional area	$A$	$10^{-5}$	m <sup>2</sup>
Beam length	$L$	1.0	m
Measurement location	$x_a$	1.0	m
Excitation location	$x_h$	1.0	m
Damping	$\zeta$	$10^{-3}$	

**Table 14.2** Experimental beam characteristics

Parameter	Value	Unit
Young's modulus	180	GPa
Density	7750	kg/m <sup>3</sup>
Approximate mass	0.056	kg
Length	0.254	m
Width	0.029	m
Height	0.001	m
Measurement location	0.010	m

## References

1. Pascual, R., Golinval, J.-C., Razeto, M.: A frequency domain correlation technique for model correlation and updating. Proceedings of the International Modal Analysis Conference—IMAC (1997)
2. Shin, K.: An alternative approach to measure similarity between two deterministic transient signals. *J. Sound Vib.* **371**, 434–445 (2016)
3. Lee, D., Ahn, T.-S., Kim, H.-S.: A metric on the similarity between two frequency response functions. *J. Sound Vib.* **436**, 32–45 (2018)
4. Manring, L.H., Schultze, J.F., Zimmerman, S.J., Mann, B.P.: Improving magnitude and phase comparison metrics for frequency response functions using cross-correlation and log-frequency shifting. *J. Sound Vib.* **539**, 117255 (2022)
5. Meirovitch, L., Parker, R.G.: Fundamentals of vibrations. *Appl. Mech. Rev.* **54**(6), B100–B101 (2001)